ZEUS-prel-06-019

Submitted to the
XXXIII International Conference on High Energy Physics
July 26 - August 2, 2006, Moscow, Russia

Abstract: **Session: QCD hard interactions**

Jet-radius dependence of inclusive-jet cross sections in the Breit frame at HERA

ZEUS Collaboration

Abstract

Differential inclusive-jet cross sections have been measured for different jet radii in neutral current deep inelastic ep scattering for boson virtualities $Q^2 > 125$ GeV^2 with the ZEUS detector at HERA using an integrated luminosity of 82 pb^{-1}. Jets were identified in the Breit frame using the k_T cluster algorithm in the longitudinally inclusive mode for three values of the jet radius R (0.5, 0.7 and 1). Differential cross sections are presented as functions of Q^2 and the jet transverse energy, $E^{\rm jet}_{T,{\rm B}}$. The jet-radius dependence of the inclusive-jet cross section has been measured for $Q^2 > 125$ and 500 GeV^2 and found to be linear with R in the range studied. Next-to-leading-order QCD calculations describe well the measurements for all the jet radii considered.

1 Introduction

The study of jet production in neutral current (NC) deep inelastic ep scattering (DIS) at HERA has been well established as a testing ground of perturbative QCD (pQCD), allowing precise determinations of α_s and its scale dependence [1–4]. Precise tests of the theory had been done at high Q^2, where Q^2 is the negative of the square of the virtuality of the exchanged boson V^* ($V = \gamma,\ Z$), by comparing the predictions at next-to-leading order (NLO) to measurements of inclusive-jet [1, 2], dijet [3, 5] and multijet [4, 6] cross sections.

The hadronic final state in NC DIS may consist of jets of high transverse energy, $E_T^{\rm jet}$, produced in the hard-scattering process. In NC DIS, the Breit frame [7] is preferred to conduct the jet search. Jet production in the Breit frame is directly sensitive to hard QCD processes. At leading order (LO) in α_s, the boson-gluon-fusion ($V^*g \rightarrow q\bar{q}$) and QCD-Compton ($V^*q \rightarrow qg$) processes give rise to two hard jets with opposite transverse momenta.

Studies of jet production at HERA have demonstrated the suitability of the k_T cluster algorithm [8] in the longitudinally invariant inclusive mode [9] as the preferred method to reconstruct jets in ep collisions. Previous analyses have always been done with jet radius $R = 1$, where R is the maximum distance in the pseudorapidity (η) - azimuth (ϕ) plane for particle recombination. However, smaller values of the jet radius R are of particular interest for the identification of heavy particles decaying into jets. NC DIS provides a well understood environment in which to study the dependence of jet production on the jet radius and to confront it with precise NLO QCD calculations in a hadron-induced reaction.

This paper presents measurements of differential inclusive-jet cross sections as a function of the jet transverse energy in the Breit frame, $E_{T,\rm B}^{\rm jet}$, and Q^2 for different values of R, namely $R = 1,\ 0.7$ and 0.5. The measurements are compared to NLO calculations [10] using currently available parameterisations of the proton parton distribution functions (PDFs).

2 Data selection and jet search

The data were collected using the ZEUS detector during the running period 1998-2000, when HERA operated with protons of energy $E_p = 920$ GeV and electrons or positrons[1] of energy $E_e = 27.5$ GeV, and correspond to an integrated luminosity of 81.7 ± 1.8 pb^{-1}.

[1] Here and in the following, the term "electron" denotes generically both the electron (e^-) and the positron (e^+), unless otherwise stated.

A detailed description of the ZEUS detector can be found elsewhere [11, 12]. Neutral current DIS events were selected offline using the same criteria as reported previously [1]. The main selection criteria are described below.

The scattered-electron candidate was identified from the pattern of energy deposits in the calorimeter (CAL) [13]. The energy (E'_e) and polar angle (θ_e) of the electron candidate were determined from the CAL measurements. The Q^2 variable was reconstructed using the double angle method ($Q^2_{\rm DA}$) [14], which uses θ_e and the angle γ_h, which corresponds to the angle of the scattered quark in the quark-parton model. The angle γ_h, defined through

$$\cos\gamma_h = \frac{(1-y)xE_p - yE_e}{(1-y)xE_p + yE_e},$$

was reconstructed using the hadronic final state [14].

The following requirements were imposed on the data sample:

- $Q^2_{\rm DA} > 125$ GeV^2;
- $|\cos\gamma_h| < 0.65$.

The k_T cluster algorithm was used in the longitudinally invariant inclusive mode to reconstruct jets in the hadronic final state both in data and in Monte Carlo (MC) simulated events (see Section 3). Three samples with different jet radii, namely $R = 1,\ 0.7$ and 0.5, were analysed. In the data, the algorithm was applied to the energy deposits measured in the CAL cells after excluding those associated with the scattered-electron candidate. The jet search was performed in the $\eta - \varphi$ plane of the Breit frame. The jet variables were defined according to the Snowmass convention [15].

After reconstructing the jet variables in the Breit frame, the massless four-momenta were boosted into the laboratory frame, where the transverse energy ($E^{\rm jet}_{\rm T,LAB}$) and the pseudorapidity ($\eta^{\rm jet}_{\rm LAB}$) of each jet were calculated. Energy corrections [1,16,17] were then applied to the jets in the laboratory frame and propagated into $E^{\rm jet}_{T,\rm B}$. The jet variables in the laboratory frame were also used to apply additional cuts on the selected sample [1]. In addition, only events with at least one jet in the pseudorapidity range $-2 < \eta^{\rm jet}_{\rm B} < 1.5$ were used for further analysis. The final data samples with at least one jet satisfying $E^{\rm jet}_{T,\rm B} > 8$ GeV contained 19917 events for $R = 1$, 16231 for $R = 0.7$ and 12935 for $R = 0.5$.

3 Monte Carlo simulation

Samples of MC events were generated to determine the response of the detector to jets of hadrons and the correction factors necessary to obtain the hadron-level jet cross sections. The hadron level is defined by those hadrons for which the lifetime is $\tau \geq 10$ ps. The generated events were passed through the GEANT 3.13-based [18] ZEUS detector- and trigger-simulation programs [12]. They were reconstructed and analysed by the same program chain as the data.

Neutral current DIS events including radiative effects were simulated using the HERACLES 4.6.1 [19] program with the DJANGOH 1.1 [20] interface to the hadronisation programs. HERACLES includes first-order corrections for initial- and final-state radiation, vertex and propagator terms, and two-boson exchange. The QCD cascade is simulated using the colour-dipole model (CDM) [21] including the leading-order (LO) QCD diagrams as implemented in ARIADNE 4.08 [22] and, as a systematic check of the final results, with the MEPS model of LEPTO 6.5 [23]. The CTEQ5D [24] parameterisations of the proton PDFs were used for these simulations. Fragmentation into hadrons is performed using the Lund string model [25] as implemented in JETSET 7.4 [26].

The jet search was performed on the MC events using the energy measured in the CAL cells in the same way as for the data. Using the sample of events generated with either ARIADNE or LEPTO-MEPS and after applying the same offline selection as for the data, a good description of the measured distributions for the kinematic and jet variables was found. The same jet algorithm was also applied to the final-state particles (hadron level) and to the partons available after the parton shower (parton level). The MC programs were also used for correcting the measured cross sections for QED radiative effects.

4 QCD calculations

The measurements were compared with LO ($\mathcal{O}(\alpha_s)$) and NLO QCD ($\mathcal{O}(\alpha_s^2)$) calculations obtained using the program DISENT [10]. The calculations were performed in the $\overline{MS}$ renormalisation and factorisation schemes using a generalised version [10] of the subtraction method [27]. The number of flavours was set to five and the renormalisation (μ_R) and factorisation (μ_F) scales were chosen to be $\mu_R = E_{T,\mathrm{B}}^{\mathrm{jet}}$ and $\mu_F = Q$, respectively. The strong coupling constant was calculated at two loops with $\Lambda_{\overline{\mathrm{MS}}}^{(5)} = 239$ MeV, corresponding to $\alpha_s(M_Z) = 0.119$. The calculations were performed using the MRST2001 [28] parameterisations of the proton PDFs. The k_T cluster algorithm was applied to the partons in the events generated by DISENT in order to compute the jet cross-section predictions.

Since the measurements refer to jets of hadrons, whereas the NLO QCD calculations refer to jets of partons, the predictions were corrected to the hadron level using the MC models. The multiplicative correction factor ($C_{\rm had}$) was defined as the ratio of the cross section for jets of hadrons over that for jets of partons, estimated by using the MC programs described in Section 3. The mean of the ratios obtained with ARIADNE and LEPTO-MEPS was taken as the value of $C_{\rm had}$. The value of $C_{\rm had}$ differs from unity by less than 5%, 15% and 25% for $R = 1$, 0.7 and 0.5, respectively, in the region $Q^2 > 500$ GeV^2. The NLO QCD predictions were also corrected for the Z^0-exchange contribution by using MC simulated events with and without Z^0-exchange.

4.1 Theoretical uncertainties

Several sources of uncertainty in the theoretical predictions were considered:

- the uncertainty on the NLO QCD calculations due to terms beyond NLO, estimated by varying μ_R by a factor of two up and down, was below $\pm 7\%$ at low Q^2 and low $E_{T,\rm B}^{\rm jet}$ and decreased to below $\pm 5\%$ for $Q^2 > 250$ GeV^2 for $R = 1$. For smaller radii the estimated uncertainty is smaller (higher) at low (high) Q^2 than for $R = 1$;
- the uncertainty on the NLO QCD calculations due to that on $\alpha_s(M_Z)$ was estimated by repeating the calculations using two additional sets of proton PDFs, MRST2001$\uparrow\uparrow$ and MRST2001$\downarrow\downarrow$ [28], determined assuming $\alpha_s(M_Z) = 0.121$ and 0.117, respectively. The difference between the calculations using these sets and MRST2001 was scaled by a factor of 1.35 to reflect the uncertainty on the world average of α_s [29]. The resulting uncertainty in the cross sections was typically below $\pm 4\%$;
- the uncertainty on the modelling of the parton shower was estimated by using half of the difference of the hadronisation corrections obtained with ARIADNE and LEPTO-MEPS. The resulting uncertainty on the cross sections was less than 1.4% for $R = 1$ and increased up to $\sim 3\%$ for smaller radii;
- the uncertainty on the NLO calculations due to those on the proton PDFs was estimated by repeating the calculations using 30 additional sets from the MRST2001 analysis [30], which takes into account the statistical and correlated systematic experimental uncertainties of each data set used in the determination of the proton PDFs. The resulting uncertainty in the cross sections was $\pm 1.6\%$ at low Q^2 and decreased to $\sim \pm 1\%$ at high Q^2;
- the uncertainty of the calculations in the value of μ_F was estimated by repeating the calculations with $\mu_F = Q/2$ and $2Q$. The variation of the calculations was negligible.

The total theoretical uncertainty was obtained by adding in quadrature the individual uncertainties listed above.

5 Acceptance corrections

Using the selected data samples of inclusive jets with $E_{T,\mathrm{B}}^{\mathrm{jet}} > 8$ GeV and $-1 < \eta_{\mathrm{B}}^{\mathrm{jet}} < 2.5$, in the kinematic region defined by $Q^2 > 125$ GeV^2 and $|\cos\gamma_h| < 0.65$, the $E_{T,\mathrm{B}}^{\mathrm{jet}}$ and Q^2 distributions were corrected bin-by-bin to the hadron level by MC techniques. For this approach to be valid, the uncorrected distributions of the data must be adequately described by the MC simulations at the detector level. This condition was in general satisfied by both ARIADNE and LEPTO-MEPS MC samples. The ARIADNE model gave a slightly better description and so it was used as the default MC for acceptance corrections; the LEPTO-MEPS samples were used as an estimate of the effect of the parton-shower model in the corrections (see Sect. 5.1). The correction factors from the ARIADNE samples differed from unity by typically less than $\sim 10\%$. These correction factors took into account the efficiency of the trigger, the selection criteria and the purity and efficiency of the jet reconstruction.

5.1 Experimental uncertainties

The following sources of systematic uncertainty were considered for the measured cross sections:

- the uncertainty in the absolute energy scale of the jets was estimated to be $\pm 1\%$ for $E_{\mathrm{T,LAB}}^{\mathrm{jet}} > 10$ GeV and $\pm 3\%$ for lower $E_{\mathrm{T,LAB}}^{\mathrm{jet}}$ values [16,31]. The resulting uncertainty on the cross sections was $\sim \pm 5\%$;
- the differences in the results obtained by using either ARIADNE or LEPTO-MEPS to correct the data for detector effects were typically below $\pm 3\%$;
- the uncertainty due to the selection cuts was estimated by varying the values of the cuts within the resolution of each variable; the effect on the cross sections was typically below $\pm 3\%$;
- the analysis was repeated using an alternative technique [32] to select the scattered-electron candidate. The resulting uncertainty was typically below $\pm 2\%$;
- the $E_{\mathrm{T,LAB}}^{\mathrm{jet}}$ cut was raised to 4 GeV. The resulting uncertainty was typically smaller than $\pm 1\%$;
- the $\eta_{\mathrm{LAB}}^{\mathrm{jet}}$ cut was set to -3 and to -1.5. The resulting uncertainty was typically below $\pm 1\%$;
- the uncertainty in the absolute energy scale of the electron candidate was estimated to be $\pm 1\%$ [33]. The resulting uncertainty was below $\pm 1\%$;

- the resulting uncertainty on the cross sections due to that in the simulation of the trigger was negligible.

The systematic uncertainties not associated with the absolute energy scale of the jets were added in quadrature to the statistical uncertainties and are shown in the figures as error bars. The uncertainty due to the absolute energy scale of the jets is shown separately as a shaded band in each figure, due to the large bin-to-bin correlation. In addition, there was an overall normalisation uncertainty of 2.2% from the luminosity determination, which is not included in the figures.

6 Results

6.1 Inclusive-jet differential cross sections for different jet radii

The inclusive-jet differential cross sections were measured in the kinematic region $Q^2 > 125$ GeV^2 and $|\cos\gamma_h| < 0.65$. These cross sections include every jet of hadrons in an event with $E_{T,\mathrm{B}}^{\mathrm{jet}} > 8$ GeV and $-2 < \eta_{\mathrm{B}}^{\mathrm{jet}} < 1.5$ and were corrected for detector and QED radiative effects.

The measurements of the inclusive-jet differential cross sections as functions of $E_{T,\mathrm{B}}^{\mathrm{jet}}$ and Q^2 are presented in Figs. 1 and 2 for different jet radii. The data points are plotted at the weighted mean in each bin of the corresponding variable. The measured $d\sigma/dE_{T,\mathrm{B}}^{\mathrm{jet}}$ ($d\sigma/dQ^2$) exhibits a steep fall-off over four (five) orders of magnitude for all jet radii in the $E_{T,\mathrm{B}}^{\mathrm{jet}}$ (Q^2) range considered.

The NLO QCD predictions are compared to the measurements in Figs. 1a and 2a. The relative difference of the measured differential cross sections to the NLO QCD calculations are shown in Figs. 1b and 2b. The calculations reproduce the measured differential cross sections well for all jet radii.

To study the scale dependence, NLO QCD calculations using $\mu_R = Q$ were also compared to the data (not shown); they also provide a good description of the data.

6.2 Dependence of the inclusive-jet cross section on the jet radius

Measurements have been performed of the inclusive-jet cross section with $E_{T,\mathrm{B}}^{\mathrm{jet}} > 8$ GeV and $-2 < \eta_{\mathrm{B}}^{\mathrm{jet}} < 1.5$ in the kinematic range given by $|\cos\gamma_h| < 0.65$ integrated above $Q^2 > 125$ and 500 GeV^2 for three different radii ($R = 1,\ 0.7$ and 0.5). The measured cross sections, $\sigma_{\rm jets}$, as functions of R are presented in Figs. 3a and b. The measured cross sections are consistent with a linear variation with R in the range between 0.5 and 1.

The predictions of LO and NLO QCD calculations of $\sigma_{\rm jets}$ are shown in the inset of Fig. 3. The LO predictions do not depend on R, since there is only one parton per jet, and exhibit a large variation with the choice of μ_R. The NLO calculations give the lowest-order non-trivial contribution to the radius dependence of the inclusive-jet cross section; for these predictions, the dependence on the choice of μ_R is largely reduced, which was studied by using calculations with either $\mu_R = E_{T,{\rm B}}^{\rm jet}$ or Q.

The NLO calculations, corrected for hadronisation and Z^0 effects, are compared to the data in Fig. 3. They give a good description of the R dependence of the data. The uncertainty of the NLO calculation with $\mu_R = E_{T,{\rm B}}^{\rm jet}$ is also shown in the figure. The total theoretical uncertainty of the cross section integrated above $Q^2 > 125$ GeV^2 (500 GeV^2) changes from 6.3% (4.7%) for $R = 1$ to 4.8% (7.7%) for $R = 0.5$. This variation is due to a change of the uncertainty due to the contribution from higher orders; the uncertainties arising from that on $\alpha_s(M_Z)$ and those on the proton PDFs do not change significantly with R.

7 Summary

Measurements of the differential cross sections for inclusive-jet production in neutral current deep inelastic ep scattering at a centre-of-mass energy of 318 GeV have been presented. The cross sections refer to jets of hadrons identified in the Breit frame with the k_T cluster algorithm in the longitudinally invariant inclusive mode. The cross sections are given in the kinematic region of $Q^2 > 125$ GeV^2 and $|\cos\gamma_h| < 0.65$.

The dependence of the inclusive-jet cross sections on the jet radius R has been studied by making measurements for $R = 0.5$, 0.7 and 1. The NLO QCD calculations provide a good description of the measured inclusive-jet differential cross sections $d\sigma/dE_{T,{\rm B}}^{\rm jet}$ and $d\sigma/dQ^2$ for all the R values considered. It is observed that the inclusive-jet cross section varies linearly with R in the range studied.

References

[1] ZEUS Coll., S. Chekanov et al., Phys. Lett. **B 547**, 164 (2002).

[2] H1 Coll., C. Adloff et al., Eur. Phys. J. **C 19**, 289 (2001).

[3] ZEUS Coll., J. Breitweg et al., Phys. Lett. **B 507**, 70 (2001).

[4] ZEUS Coll., S. Chekanov et al., Eur. Phys. J. **C 44**, 183 (2005).

[5] H1 Coll., C. Adloff et al., Eur. Phys. J. **C 19**, 429 (2001).

[6] H1 Coll., C. Adloff et al., Phys. Lett. **B 515**, 17 (2001).

[7] R.P. Feynman, *Photon-Hadron Interactions*. Benjamin, New York, (1972);
K.H. Streng, T.F. Walsh and P.M. Zerwas, Z. Phys. **C 2**, 237 (1979).

[8] S. Catani et al., Nucl. Phys. **B 406**, 187 (1993).

[9] S.D. Ellis and D.E. Soper, Phys. Rev. **D 48**, 3160 (1993).

[10] S. Catani and M.H. Seymour, Nucl. Phys. **B 485**, 291 (1997). Erratum in Nucl. Phys. **B 510**, 503 (1998).

[11] ZEUS Coll., M. Derrick et al., Phys. Lett. **B 293**, 465 (1992).

[12] ZEUS Coll., U. Holm (ed.), *The ZEUS Detector*. Status Report (unpublished), DESY (1993), available on `http://www-zeus.desy.de/bluebook/bluebook.html`.

[13] H. Abramowicz, A. Caldwell and R. Sinkus, Nucl. Inst. Meth. **A 365**, 508 (1995);
R. Sinkus and T. Voss, Nucl. Inst. Meth. **A 391**, 360 (1997).

[14] S. Bentvelsen, J. Engelen and P. Kooijman, *Proc. of the Workshop on Physics at HERA*, W. Buchmüller and G. Ingelman (eds.), Vol. 1, p. 23. Hamburg, Germany, DESY (1992);
K.C. Höger, ibid., p. 43.

[15] J.E. Huth et al., *Research Directions for the Decade. Proc. of Summer Study on High Energy Physics, 1990*, E.L. Berger (ed.), p. 134. World Scientific (1992). Also in preprint FERMILAB-CONF-90-249-E.

[16] ZEUS Coll., S. Chekanov et al., Phys. Lett. **B 531**, 9 (2002).

[17] ZEUS Coll., S. Chekanov et al., Phys. Lett. **B 558**, 41 (2003).

[18] R. Brun et al., GEANT3, Technical Report CERN-DD/EE/84-1, CERN, 1987.

[19] A. Kwiatkowski, H. Spiesberger and H.-J. Möhring, Comp. Phys. Comm. **69**, 155 (1992);
H. Spiesberger, *An Event Generator for ep Interactions at HERA Including Radiative Processes (Version 4.6)*, 1996, available on `http://www.desy.de/~hspiesb/heracles.html`.

[20] K. Charchuła, G.A. Schuler and H. Spiesberger, Comp. Phys. Comm. **81**, 381 (1994);
H. Spiesberger, HERACLES *and* DJANGOH*: Event Generation for ep Interactions at HERA Including Radiative Processes*, 1998, available on `http://www.desy.de/~hspiesb/djangoh.html`.

[21] Y. Azimov et al., Phys. Lett. **B 165**, 147 (1985);
G. Gustafson, Phys. Lett. **B 175**, 453 (1986);
G. Gustafson and U. Pettersson, Nucl. Phys. **B 306**, 746 (1988);
B. Andersson et al., Z. Phys. **C 43**, 625 (1989).

[22] L. Lönnblad, Comp. Phys. Comm. **71**, 15 (1992);
L. Lönnblad, Z. Phys. **C 65**, 285 (1995).

[23] G. Ingelman, A. Edin and J. Rathsman, Comp. Phys. Comm. **101**, 108 (1997).

[24] H.L. Lai et al., Eur. Phys. J. **C 12**, 375 (2000).

[25] B. Andersson et al., Phys. Rep. **97**, 31 (1983).

[26] T. Sjöstrand, Comp. Phys. Comm. **82**, 74 (1994);
T. Sjöstrand, Comp. Phys. Comm. **39**, 347 (1986);
T. Sjöstrand and M. Bengtsson, Comp. Phys. Comm. **43**, 367 (1987).

[27] R.K. Ellis, D.A. Ross and A.E. Terrano, Nucl. Phys. **B 178**, 421 (1981).

[28] A.D. Martin et al., Eur. Phys. J. **C 23**, 73 (2002).

[29] S. Bethke, J. Phys. **G 26**, R27 (2000). Updated in Preprint hep-ex/0407021, 2004.

[30] A.D. Martin et al., Eur. Phys. J. **C 28**, 455 (2003).

[31] ZEUS Coll., S. Chekanov et al., Eur. Phys. J. **C 23**, 615 (2002);
M. Wing (on behalf of the ZEUS Coll.), *Proc. of the 10th International Conference on Calorimetry in High Energy Physics*, R. Zhu (ed.), p. 767. Pasadena, USA (2002). Also in preprint hep-ex/0206036.

[32] ZEUS Coll., J. Breitweg et al., Eur. Phys. J. **C 11**, 427 (1999).

[33] ZEUS Coll., S. Chekanov et al., Eur. Phys. J. **C 21**, 443 (2001).

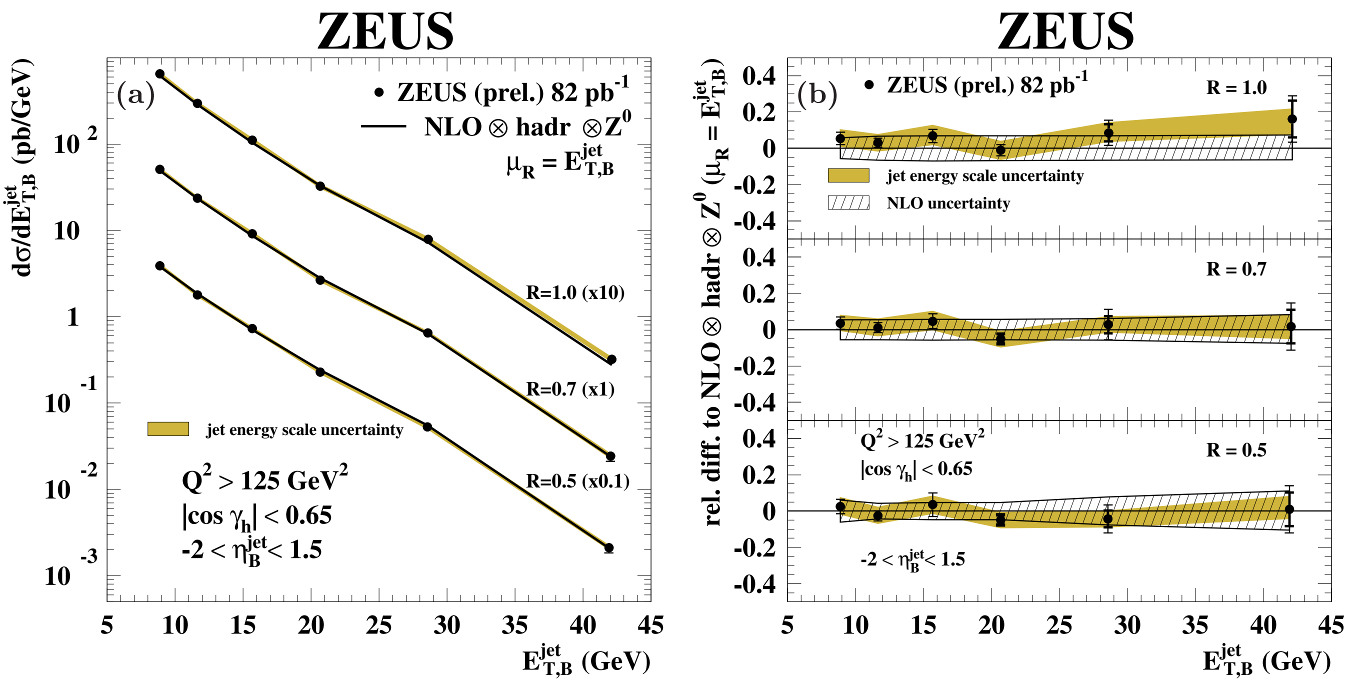

Figure 1: *(a) The measured differential cross-section $d\sigma/dE_T^{\rm jet}$ for inclusive-jet production with $-2 < \eta_{\rm B}^{\rm jet} < 1.5$ (dots) for different jet radii, in the kinematic range given by $Q^2 > 125$ GeV^2 and $|\cos\gamma_h| < 0.65$. The inner error bars represent the statistical uncertainty. The outer error bars show the statistical and systematic uncertainties, not associated with the uncertainty in the absolute energy scale of the jets, added in quadrature. The shaded bands display the uncertainty due to the absolute energy scale of the jets. The NLO QCD calculations with $\mu_R = E_{T,\rm B}^{\rm jet}$ (solid lines), corrected for hadronisation and Z^0 effects and using the MRST2001 parameterisations of the proton PDFs, are also shown. Each cross section has been multiplied by the scale factor indicated in brackets to aid visibility. (b) The fractional differences between the measured $d\sigma/dE_T^{\rm jet}$ and the NLO QCD calculations with $\mu_R = E_{T,\rm B}^{\rm jet}$ (dots); the hatched bands display the total theoretical uncertainty.*

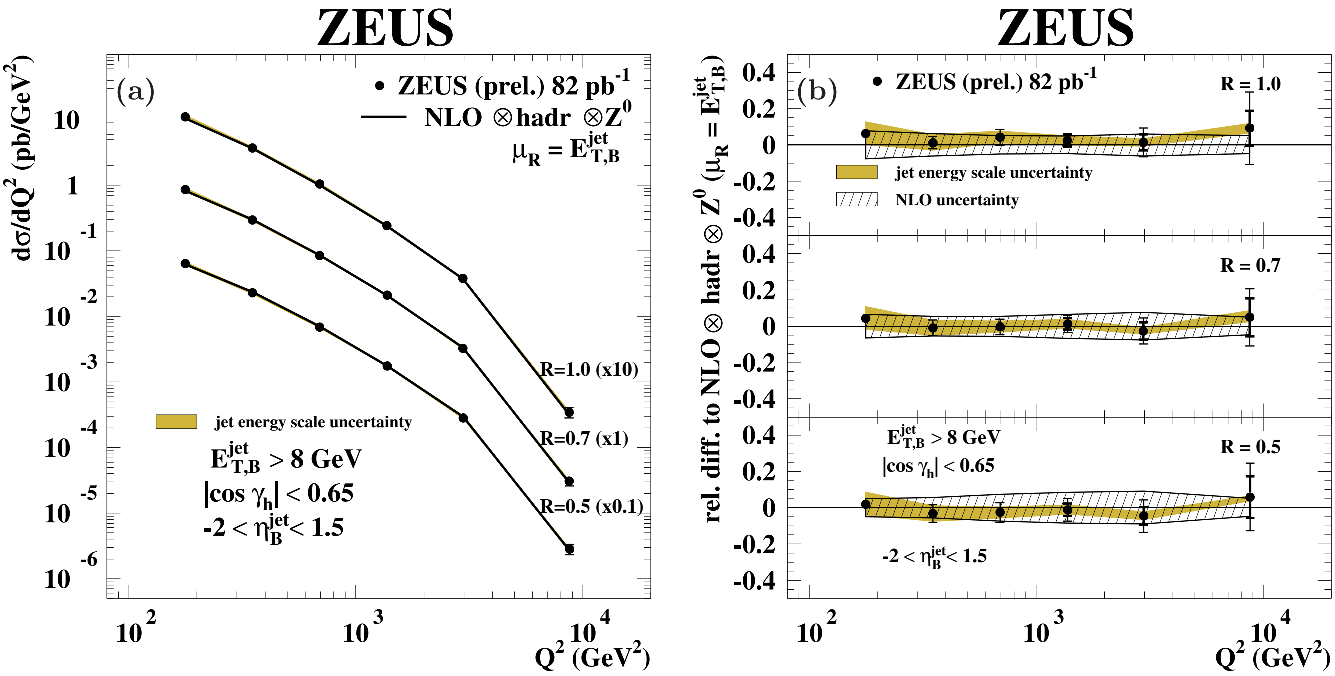

Figure 2: *The measured differential cross-section $d\sigma/dQ^2$ for inclusive-jet production with $E_{T,\mathrm{B}}^{\mathrm{jet}} > 8$ GeV and $-2 < \eta_{\mathrm{B}}^{\mathrm{jet}} < 1.5$ (dots) for different jet radii, in the kinematic range given by $|\cos\gamma_h| < 0.65$. Other details as in the caption to Fig. 1.*

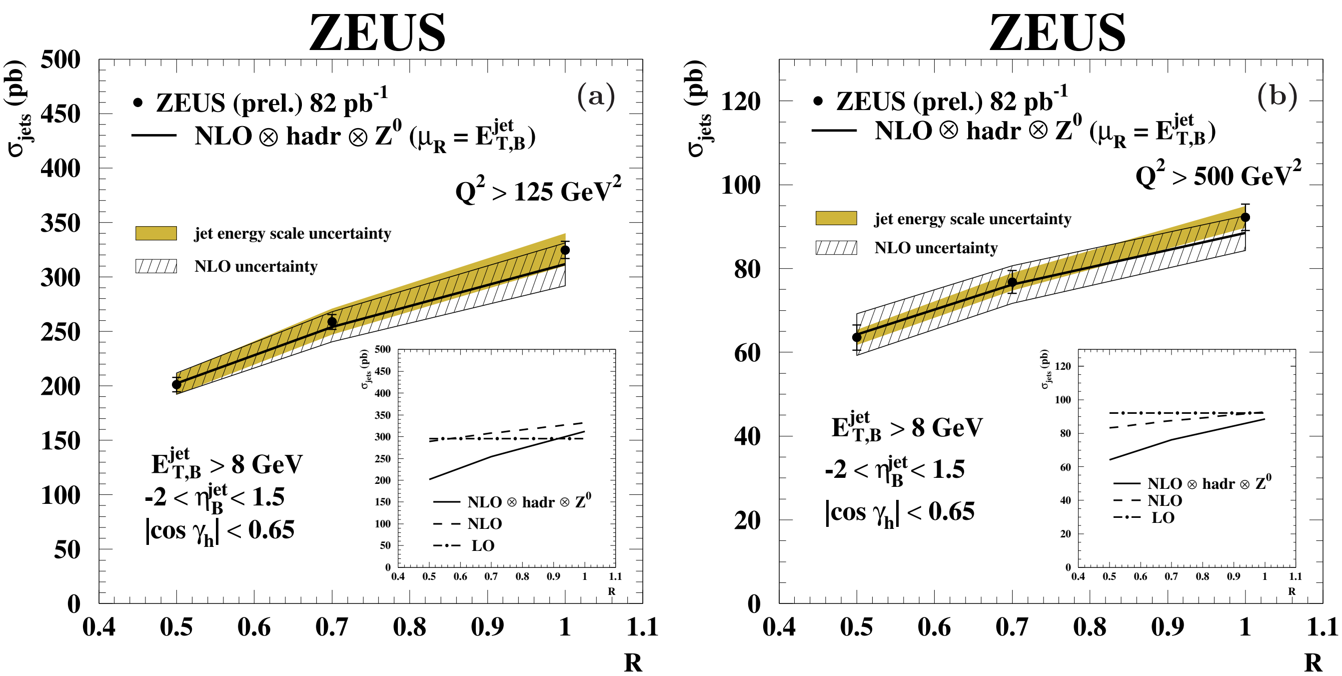

Figure 3: *The measured cross-section $\sigma_{\rm jets}$ as a function of the jet radius for inclusive-jet production with $E^{\rm jet}_{T,{\rm B}} > 8$ GeV and $-2 < \eta^{\rm jet}_{\rm B} < 1.5$ (dots), in the kinematic range given by $|\cos\gamma_h| < 0.65$ and (a) $Q^2 > 125$ GeV^2 and (b) $Q^2 > 500$ GeV^2. The insets show the LO (dot-dashed lines) and NLO (dashed lines) QCD calculations with $\mu_R = E^{\rm jet}_{T,{\rm B}}$. The NLO QCD calculations corrected for hadronisation and Z^0 effects are shown as solid lines. Other details as in the caption to Fig. 1.*